

Electrical impedance and electric modulus approach of double perovskite $\text{Pr}_2\text{ZnZrO}_6$ ceramics

Dev K. Mahato · T. P. Sinha

Received: 27 June 2013 / Accepted: 23 July 2013 / Published online: 3 August 2013
© Springer Science+Business Media New York 2013

Abstract The polycrystalline praseodymium zinc zirconate $\text{Pr}_2\text{ZnZrO}_6$ (PZZO) is synthesized at 1,150 °C by means of solid state reaction technique. X-ray structural analysis confirmed the formation of a single phase monoclinic structure at room temperature. The nonzero intercept in the Nyquist plot indicates the presence of an arc for frequency higher than the maximum frequency measured (1 MHz). Comparative study of the impedance and modulus plot confirm the contribution from grain and grain-boundary and grain-boundary contribution dominates in the material. The activation energy of the compound calculated from imaginary part of impedance plot is found to be 0.442 eV which suggests that the polaron hopping is responsible for conduction mechanism in PZZO. Semiconducting behavior of the material is observed. Summerfield scaling shows a quite satisfying overlap of the data at different temperatures on a single master curve.

1 Introduction

Electronic circuit technologies have been developed with the support of the research and development of many materials including dielectric and magnetic substances. With the rapid development of microelectronic devices such as capacitors, resonators and filters, research on perovskite type compounds have been on an increasing

demand. Perovskite compounds with general formula ABO_3 show a large variety of interesting functional properties such as ferro/piezo/pyro-electricity, magnetic order, colossal magnetoresistance, superconductivity etc. due to their compositional and structural diversity [1–4]. One of the major characteristic of perovskites is the possibility of multiple substitution of cations at the A- and B-site of the ABO_3 unit cell. When the ideal perovskite formula ABO_3 is change to introduce two different types of cations on the octahedral site of the perovskite unit cell, the cationic ordering leads to a cubic complex superstructure perovskite corresponds to well-known formula $\text{A}_2\text{B}'\text{B}''\text{O}_6$.

Double perovskites having general formula $\text{A}_2\text{B}'\text{B}''\text{O}_6$ and related materials are among inorganic compounds of great interest due to their large variety of physical properties and technological application [5–7] based on the different elements A, B' and B'' that can be accommodated in the structure. Double perovskites $\text{A}_2\text{B}'\text{B}''\text{O}_6$ host two different B-site cations, which tend to order in a NaCl-type super lattice structure, doubling the ABO_3 perovskite cell [8]. It is especially interesting in view of the possibility that B' and B'' cations could be ordered at the octahedral sites, giving rise to novel electrical and magnetic properties. In $\text{A}_2\text{B}'\text{B}''\text{O}_6$, A represents a alkaline earth metal or rare earth ions of larger ionic radii, B' and B'' octahedral sites are occupied alternately by different transition metal cations with smaller ionic radii. Double perovskite became of technological interest when the search for ferroelectric and piezoelectric materials, for mainly capacitor application, was extended from the common perovskite ABO_3 to more complex systems so called double perovskites $\text{A}_2\text{B}'\text{B}''\text{O}_6$. Efforts to explore new candidate double perovskites with improved properties are still highly desirable. We are especially interested with the subgroup of these compounds where B' and B'' are the transition metal cations of 3d and

D. K. Mahato (✉)
Department of Physics, National Institute of Technology, Patna,
Patna 800 005, India
e-mail: drdevkumar@yahoo.com

T. P. Sinha
Department of Physics, Bose Institute, 93/1, Acharya Prafulla
Chandra Road, Kolkata 700 009, India

4d electronic configuration respectively. Previous studies have shown that the $3d^0$ cations of smaller ionic radii have higher polarizability in a lattice. Some new double perovskite oxides have investigated for their relatively low dielectric properties with low loss values [9]. From the electrical point of view, polarization needs transition metals with filled 3d orbitals. Previous reports [9, 10] shows most of the double perovskites have a transition metal ions as one of the B-cations. It is therefore interesting to study the electrical properties of double perovskites with closed shell ions (i.e. Zn^{2+} , filled 3d orbitals) as one of the B-cations, which would make the material poor conductor.

To the best of our knowledge, there are no reports on physical properties of the Pr_2ZnZrO_6 double perovskite in spite of a large number of work that has been done on double perovskite. In the present work we describe the electric impedance and electric modulus of a new double perovskite oxide Pr_2ZnZrO_6 in a wide range of frequency (90 Hz–1 MHz) at various temperatures by impedance spectroscopy. An ac impedance spectroscopy is a useful technique to analyze the electrical properties of ceramic materials such as the determination of relaxation frequency and separation of grain, grain boundary and grain-electrode effects.

2 Experimental procedure

Pr_2ZnZrO_6 polycrystalline sample was synthesized by conventional solid state reaction method using high purity Pr_2O_3 , ZnO and ZrO_2 and stoichiometrically mixed in a agate mortar in the presence of acetone (Merck) for 12 h. The mixture was calcined in a Pt crucible at 1,100 °C in air for 10 h and brought to room temperature at a cooling rate of 100 °C/h. The calcined sample was palletized into a circular disc using PVA as binder which was burnt out during sintering at 1,150 °C for 6 h, and cooled slowly to room temperature at a cooling rate 1 °C/min. The sample was characterized by X-ray diffraction pattern. The X-ray diffractogram of the sample was recorded at room temperature with powder X-ray diffractometer (Rigaku Miniflex-II) with $CuK\alpha$ radiation. The scanning electron microscope (SEM) (FEI Quanta 200) equipped with energy dispersive analysis of X-ray (EDAX) is used to determine the grain size distribution, the atomic composition and homogeneity of the sample. The sintered pellets were polished to make both their faces parallel and electroded by high purity ultrafine silver paste for all their electrical characterization. To dry the paste the pellets were heated at 500 °C for 2 h prior to conducting experiment. Capacitance, impedance, phase and conductance of the sample were measured as a function of frequency and temperature using a computer controlled LCR-meter (HIOKI-3552, Japan) at a heating rate of 0.5 °C/min.

The Eurotherm 2216e temperature controller was used to control the temperature of the sample.

3 Results and discussion

3.1 Structural characterization

The X-ray diffraction pattern obtained at room temperature for the polycrystalline PZZO prepared by solid-state reaction route is shown in Fig. 1. All the diffraction peaks of the X-ray profile could be indexed to a monoclinic cell and lattice parameters were determined using a least-squares method with the help of a standard computer programme (Crysfire). The cell parameters of the compound crystallized in monoclinic phase at room temperature are: $a = 7.842564 \pm 0.004956$ Å, $b = 6.238330 \pm 0.001626$ Å, $c = 6.085978 \pm 0.00187$ Å, $\beta = 97.9232^\circ \pm 0.00187^\circ$ with cell volume = 294.91 Å³. SEM image of fractured surface of the sample is shown in Fig. 2. The average grain size of PZZO is found to be 0.85 μm. The survey spectrum obtained by EDAX is shown in Fig. 3. Well resolved lines originating from the constituents atoms are recorded in a wide energy range. The composition calculated for the entire surface area is listed in the table (inset of Fig. 3). The EDAX spectrum confirms the homogeneity of the sample.

3.2 Impedance analysis and electric modulus formalism

Angular frequency dependence of the real part (Z') of complex impedance Z^* ($=Z' + iZ''$) of Pr_2ZnZrO_6 at various temperatures is shown in Fig. 4. The variation of Z' with frequency for all temperatures implies relaxation process in the sample. The magnitude of Z' decreases with

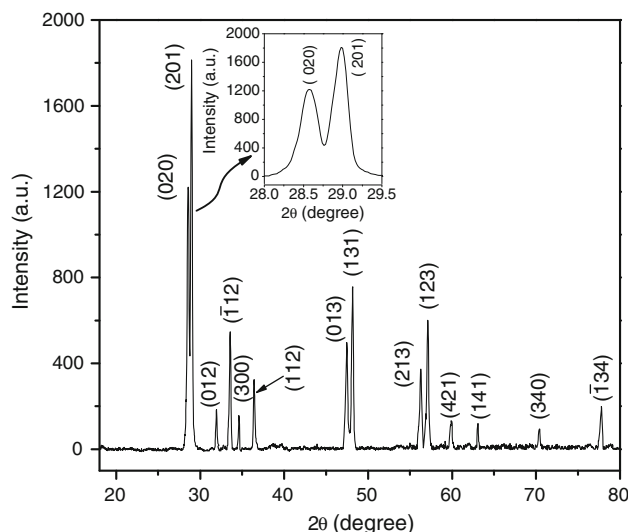


Fig. 1 XRD diffraction pattern of Pr_2ZnZrO_6 at room temperature

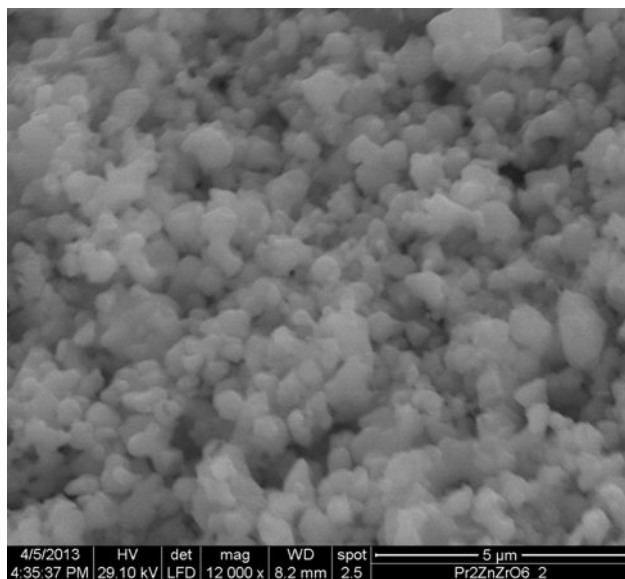


Fig. 2 SEM image of fracture surface of Pr₂ZnZrO₆ sintered pellet

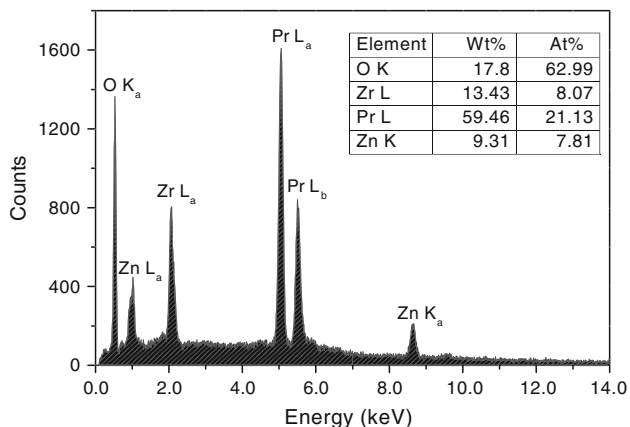


Fig. 3 Survey spectrum of EDAX for Pr₂ZnZrO₆

increasing temperature at lower frequency indicates increase in the ac conductivity in PZZO. The Z' values merge at higher frequencies for all temperatures indicating release of space charges as a result of reduction in the barrier properties of the material. Figure 5 shows angular frequency dependence of the imaginary part (Z'') of complex impedance Z^* of Pr₂ZnZrO₆ at various temperatures. Both the real and imaginary parts of impedance strongly depend on frequency at different temperatures. The curves in Fig. 5 show that maxima peak (Z''_m) shifts to higher frequencies on increasing temperature indicating that resistance of the bulk material is decreasing and a strong dispersion of Z'' exists. The total resistance (impedance) decreases with an increase in temperature across entire frequency range showing semi conducting behavior. Fitting of the impedance data was performed with Cole–Cole relation:

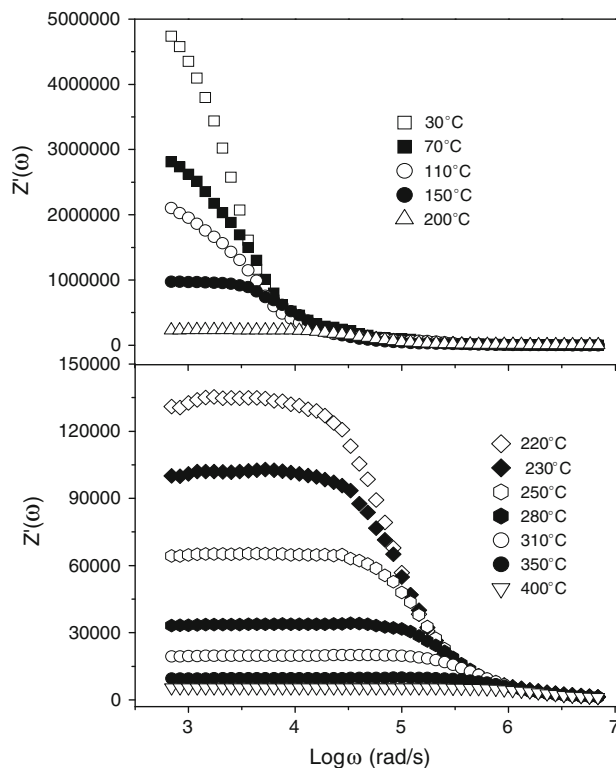


Fig. 4 Angular frequency dependence of the real part (Z') of impedance of Pr₂ZnZrO₆ at various temperatures

$$Z^* = R_\infty + (R_0 - R_\infty) / [1 + (j\omega\tau_c)^\alpha] \quad (1)$$

where R_0 and R_∞ are the resistances at very low and very high frequencies, respectively, τ_c is the characteristic relaxation time of the system corresponding to the characteristic angular frequency ω at the peak position of Z'' in the Z'' versus $\log\omega$ plot and α is the dimensionless exponent that denotes the angle of tilt of the circular arc from the real axis. The best fitting of the impedance data with Eq. (1) is shown by solid lines in Fig. 5 for Z'' . The value of α lies between 0.72 and 0.76.

The width of the peak in the Fig. 5 points towards the possibility of a distribution of relaxation times. The most probable relaxation time $\tau_m (=1/\omega_m)$ from the position of the peak in the Z'' versus $\log\omega$ plots can be determined. The most probable relaxation time follows the Arrhenius law given by the relation: $\omega_m = \omega_0 \exp(-E_a/k_B T)$.

A plot of the $\log\omega_m$ versus inverse of absolute temperature ($1/T$) is shown in the inset of Fig. 6. The activation energy E_a calculated from the least-squares fit to the points is 0.484 eV. The scaling behavior of Z'' clearly indicates that the relaxation mechanism is nearly temperature independent (Fig. 6).

Figure 7 illustrates a set of impedance data taken over a wide frequency range at several temperatures as a Nyquist plot (Z'' vs Z') for PZZO sample. Usually, the conductivity

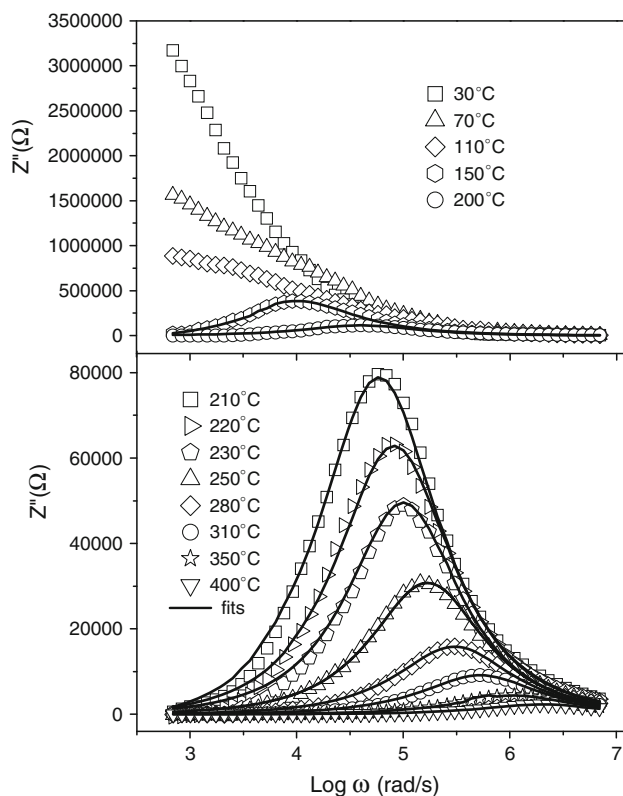


Fig. 5 Angular frequency dependence of the imaginary part (Z'') of impedance of $\text{Pr}_2\text{ZnZrO}_6$ at various temperatures. The *solid lines* are fits of the impedance curves

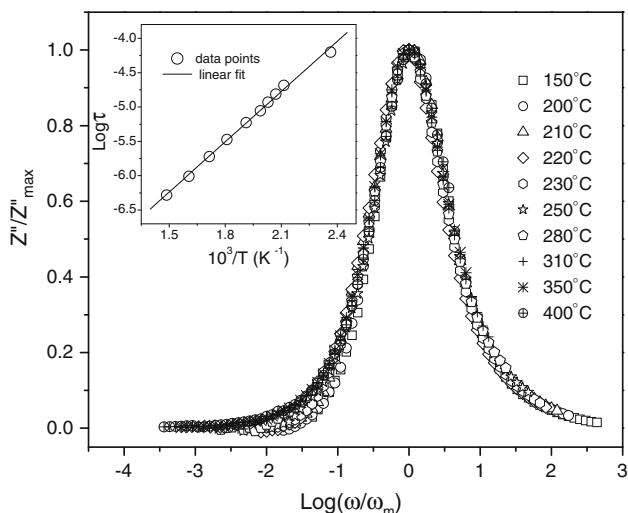


Fig. 6 Scaling behaviour of Z'' at various temperatures of $\text{Pr}_2\text{ZnZrO}_6$. The temperature dependence of the most probable relaxation frequency is shown in the *inset* where the *symbols* are the experimental points and the *solid line* is the least-squares straight line fit

of oxide materials is highly dependent upon both the carrier concentration and mobility. It is observed that the centre of the semicircular arc shifts towards the origin on increasing

temperature which indicates that the conductivity of the samples increases with increase in temperature. In the impedance spectrum, only single semicircular arcs (hollow curves) are observed at all temperatures with nonzero intercept at high frequencies (not shown here) indicate that the sample is electrical inhomogeneous. Single semicircular arcs observed in the complex impedance plane at lower frequencies reveal that the conduction in the material is predominant in grain boundary [11]. The nonzero intercept indicates the presence of an arc for frequency higher than the maximum frequency measured (1 MHz), which is assigned as the contribution from grain interior while the large semicircular arc at low frequencies originates from the grain boundaries. In other words, this semicircle is ascribed to originate from the grain boundary and nonzero intercept corresponding to the resistance of the grain, with no semicircle corresponding to electrode-sample interface [12]. There is a relaxation relating to the grain boundary which is probably due to a Schottky-type barrier existing in this type of polycrystalline material. The resistances of grain and grain boundaries can be estimated from the intercepts of the curves with the X-axis i.e. with the real part of the impedance Z' axis. The grain resistance (R_g), grain boundary resistance (R_{gb}) and grain boundary capacitances (C_{gb}) values at 150, 180, 200, 220 and 250 °C are shown in Table 1. The corresponding values of the resistivities of grain (ρ_g) and grain boundary (ρ_{gb}) are 52.26, 58.25, 62.76, 65.50, 67.44 and 46,502.53, 18,583.54, 10,992.61, 6,261.384, 3,073.52 Ωm respectively.

Figure 8 shows a complex impedance plane plot of PZZO compound and the corresponding equivalent circuit (inset of Fig. 8) at different temperatures. The values of grain and grain-boundary resistances and capacitances can be obtained by an equivalent circuit of two parallel resistance–capacitance (RC) elements connected in series. The equivalent electrical equations for grain and grain boundary are

$$Z' = R_s + \frac{R_g}{1 + (\omega R_g C_g)^2} + \frac{R_{gb}}{1 + (\omega R_{gb} C_{gb})^2} \quad (2)$$

and

$$Z'' = R_g \left[\frac{\omega R_g C_g}{1 + (\omega R_g C_g)^2} \right] + R_{gb} \left[\frac{\omega R_{gb} C_{gb}}{1 + (\omega R_{gb} C_{gb})^2} \right] \quad (3)$$

where C_g and C_{gb} are the grain and grain-boundary capacitances and R_g and R_{gb} are the grain and grain-boundary resistances. We have fitted our experimental data with Eqs. (2) and (3) as shown by solid lines in Fig. 8.

Electric modulus formalism M^* ($=M' + iM''$, where M' and M'' are the real and imaginary part of M^* respectively) is an alternative approach to explore the dynamical aspects of electrical transport phenomena of materials. Although

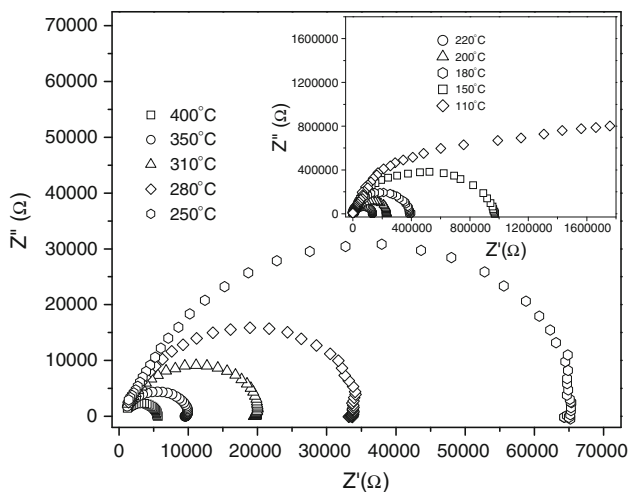


Fig. 7 Complex-plane impedance plots for $\text{Pr}_2\text{ZnZrO}_6$ at various temperatures

Table 1 As obtained from the intercept of the semicircles with the x -axis the values of R_{gb} and R_g and corresponding C_{gb} values

Temp (°C)	R_{gb} (Ω)	C_{gb} (F)	R_g (Ω)
150	972,856.36	9.3442×10^{-11}	1,093.25
180	388,776.99	9.3087×10^{-11}	1,218.59
200	229,970.98	1.0887×10^{-10}	1,313.03
220	130,991.307	1.0999×10^{-10}	1,370.32
250	64,299.68	1.0725×10^{-10}	1,410.84

M^* was originally introduced to study space charge relaxation phenomena [13], it is now widely used to analyze ionic conductivities [14]. The Argand diagram for electric modulus (M'' vs M') of $\text{Pr}_2\text{ZnZrO}_6$ at 150 °C temperatures is shown in Fig. 9. In order to confirm the ambiguity arising due to the presence of grain/grain boundary effect [15] at elevated temperatures, the impedance data are re-plotted in the modulus formalism. It is clear that the modulus plane plots exhibit two semicircles of unequal sizes: one corresponds to grain and other grain boundary.

As an alternate approach to confirm the presence of grain and/or grain boundary effect, the same impedance data can be analyzed much better by re-plotting them in the form of spectroscopic plot of Z'' and imaginary part of complex modulus M'' as shown in Fig. 10 at the same temperature 150 °C. The Z'' plot contains a single peak corresponding to a semicircle while M'' plot shows two peaks. The higher frequency M'' peak represents a bulk component of the sample. The single peak of Z'' corresponding to the lower frequency of the two M'' peaks explained the equivalent circuits at these temperatures. Appears to contain two parallel RC elements—the

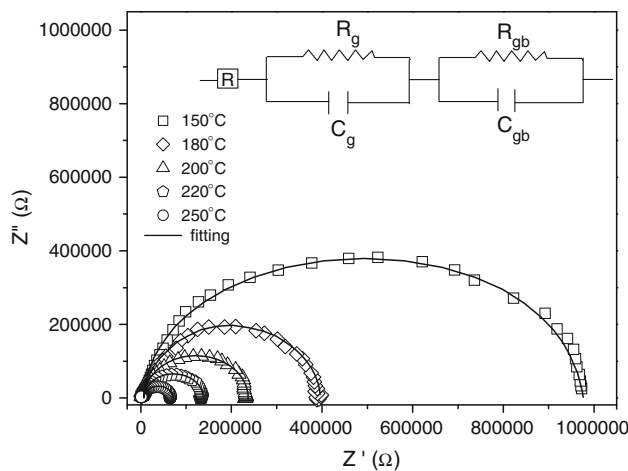


Fig. 8 Complex impedance spectrum of $\text{Pr}_2\text{ZnZrO}_6$ at 150, 180, 200, 220 and 250 °C temperatures. *Solid line* is the fitting to the experimental data by RC equivalent circuit

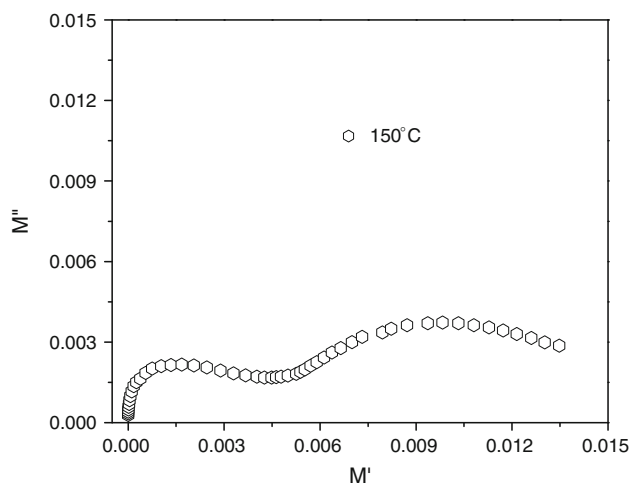


Fig. 9 Argand diagram for electric modulus (M'' vs M') of $\text{Pr}_2\text{ZnZrO}_6$ at 150 °C temperatures

resistance of one is much lower than that of the other, but the two capacitance values are not too dissimilar.

The angular frequency dependence of the electric modulus M' and M'' of PZZO at various temperatures is shown in Fig. 11. The sample shows a two step increase in M' in the measured frequency range. Correspondingly, M'' shows two peaks in the same frequency range, both peaks shift to higher frequency with increasing temperature. These peaks indicate the transition from short range to long range mobility with decreasing frequency, where the low frequency side of the peak represents the range of frequencies in which the ions are capable of moving long distances i.e. performing hopping from one site to the neighboring site, whereas for the high frequency side the ions are spatially confined to their potential wells and can execute only localized motion [16].

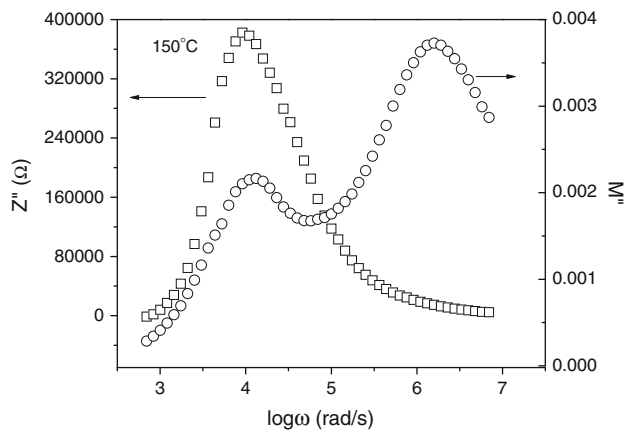


Fig. 10 Spectroscopic plot of Z'' and M'' for $\text{Pr}_2\text{ZnZrO}_6$ at 150°C temperature

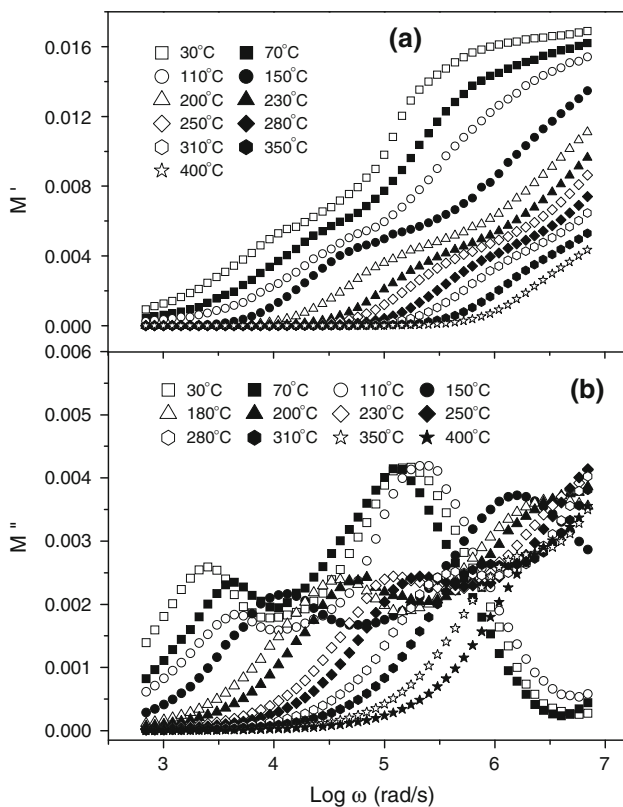


Fig. 11 Frequency dependence of **a** M' and **b** M'' of $\text{Pr}_2\text{ZnZrO}_6$ at various temperatures

3.3 AC conductivity study

The frequency dependence of ac conductivity (σ_{ac}) for PZZO at various temperatures is shown in Fig. 12. The conductivity spectra show plateaus at low frequencies and high temperatures i.e. above 200°C (i.e. conductivity does not depend on frequency) which corresponds to the dc conductivity (σ_{dc}). The value of σ_{dc} is found to increase

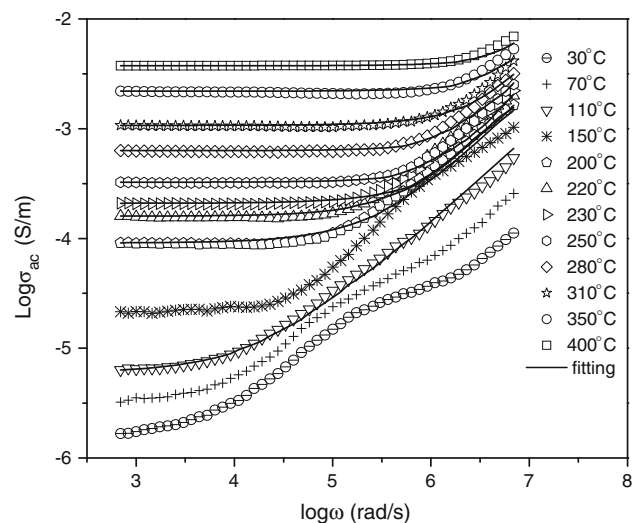


Fig. 12 Frequency dependence ac conductivity (σ_{ac}) of $\text{Pr}_2\text{ZnZrO}_6$ at various temperatures where the symbols are the experimental points and the *solid lines* represent the fitting to Eq. (4)

with an increase of temperature showing the semiconducting behavior of the material. A strong dispersion is observed at higher frequency region for lower temperatures. The conductivity spectra follow the Jonscher power law [17] defined as:

$$\sigma = \sigma_{dc} \left[1 + \left(\frac{\omega}{\omega_H} \right)^n \right] \quad (4)$$

where ω_H is the hopping frequency of charge carriers, and n is the dimensionless frequency exponent. The experimental conductivity data of PZZO are fitted to Eq. (4) with σ_{dc} and ω_H as variables keeping in mind that the values of parameter n are weakly temperature dependent. The best fit of conductivity spectra is shown by solid lines in Fig. 11 at various temperatures. The reciprocal temperature dependence of σ_{dc} is shown in the inset of Fig. 13 which follows Arrhenius law with an activation energy of 0.480 eV. Such a value of activation energy suggests that the conduction mechanism in PZZO may be due to the hopping of small polaron between neighboring sites within the crystal lattice and are consistent with our earlier reports [18, 19]. In highly polarizable lattices like oxides perovskites electronic localization results in a lattice deformation and polarization. Since such polarons are carrying a charge, an electronic dipole moment and an elastic energy.

Figure 13 shows $\log(\sigma_{ac}/\sigma_{dc})$ versus $\log(\omega/\sigma_{dc}T)$ plot at different temperatures for PZZO. This so-called Summerfield scaling [20, 21] uses the directly measurable quantities σ_{dc} and T as the scaling parameter. From Fig. 13, it is obviously seen that a quite satisfying overlap of the data at different temperatures on a single master curve illustrates well the dynamic processes occurring at different frequencies need almost the same thermal activation energy.

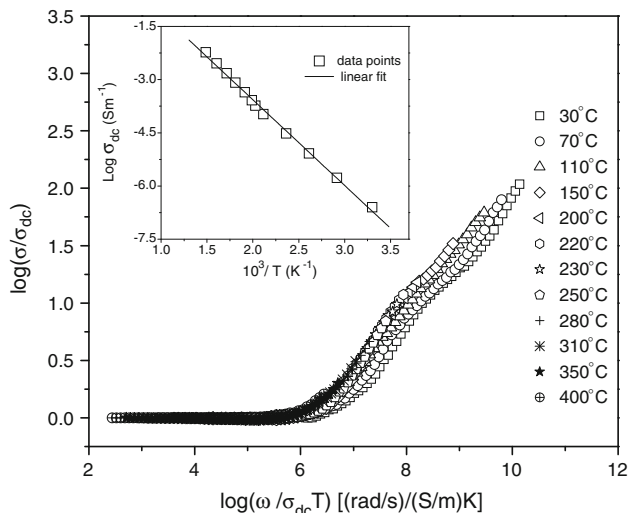


Fig. 13 Summerfield scaling for conductivity spectra at different temperatures of $\text{Pr}_2\text{ZnZrO}_6$. *Inset* The temperature dependence of dc conductivity curve for $\text{Pr}_2\text{ZnZrO}_6$, where the symbols are the experimental points and the *solid line* is the least-squares straight line fit

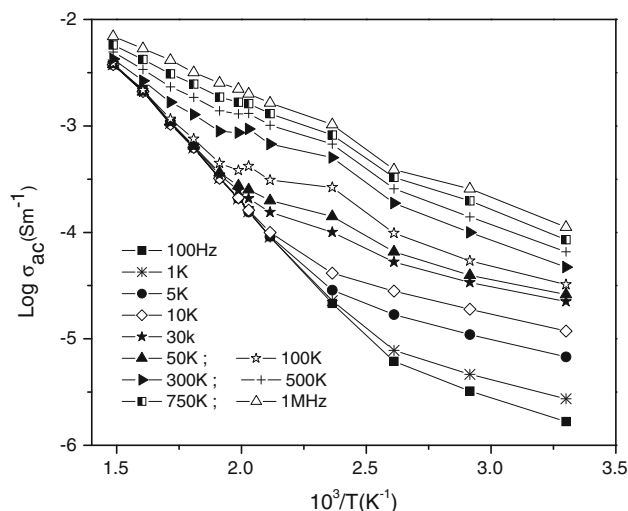


Fig. 14 Reciprocal temperature dependence of ac conductivity for $\text{Pr}_2\text{ZnZrO}_6$ at different frequencies

Another indication of those scaled master curves is that all Arrhenius temperature dependence of conductivity is embedded in the dc conductivity term.

Reciprocal temperature dependence of ac conductivity is shown in Fig. 14. Ac conductivity activation energy decreases with increasing frequency and different activation energies (0.36–0.48 eV) involved in different temperature regions in the conduction process.

4 Conclusions

The PZZO compound was electrically characterized by impedance spectroscopy in a wide frequency range at

various temperatures. XRD study revealed a room temperature monoclinic phase. The nonzero intercept in impedance plane plot indicates the presence of an arc at higher frequency corresponding to the grain properties followed by a second large semicircular arc attributed to the grain boundary. Single semicircular arcs observed at lower frequencies reveal that the conduction in the material is predominant in grain boundary. Activation energy shows that the conduction mechanism in PZZO may be due to the polaron hopping. The dc conductivity was found to increase with an increase of temperature showing the semiconducting behavior of the material. Summerfield scaling behavior illustrated that all Arrhenius temperature dependence of conductivity was embedded in the dc conductivity term.

Acknowledgments This work is financially supported by Defence Research Development Organisation, Government of India, New Delhi.

References

1. E.J. Baran, *Catal. Today* **8**, 122 (1990)
2. I. Kuzmanovski, S. Dimitrovska-Lazova, S. Aleksavska, *Anal. Chim. Acta* **595**, 182 (2007)
3. F.S. Galasso (ed.), *Structure, Properties and Preparation of Perovskite type Compounds* (Pergamon Press, Oxford, 1969)
4. J.F. Marucco, *Chimie des Solides* (EDP Sciences, Les Ulis, 2004)
5. B. Garcia-Landa, C. Ritter, M.R. Ibarra, J. Blasco, P.A. Algarabel, R. Mahaenderon, J. Garcia, *Solid State Commun.* **110**, 435 (1999)
6. E. Burzo, I. Balaszo, M. Albu, *Rev. Chim. (Buchrest)* **59**(11), 1205 (2008)
7. L.C. Chioaru, I. Jitaru, M. Bicher, V. Matei, O. Mihai, *Rev. Chim. (Buchrest)* **60**(3), 283 (2009)
8. D. Iwanaga, Y. Inaguma, M. Itoh, *J. Solid State Chem.* **147**, 291 (1999)
9. A.K. Ganguli, V. Grover, M. Thirumal, *Mater. Res. Bull.* **36**, 1967 (2001)
10. M.T. Anderson, K.B. Greenwood, L.A. Taylor, K.R. Poeppelmeier, *Prog. Solid State Chem.* **22**, 197 (1993)
11. D.K. Mahato, A. Dutta, T.P. Sinha, *J. Mater. Sci.* **45**, 6757 (2010)
12. L. Fang, M.R. Shen, Z.Y. Li, W.W. Cao, *Chin. Phys. Lett.* **23**(4), 990 (2006)
13. P.B. Macedo, C.T. Moynihan, R. Bose, *Phys. Chem. Glasses* **13**, 17 (1972)
14. C.A. Angell, *Chem. Rev.* **90**, 523 (1990)
15. R.N.P. Choudhary, D.K. Pradhan, C.M. Tirado, G.E. Bonilla, R.S. Katiyar, *Phys. Status Solidi (b)* **244**, 2254 (2007)
16. J.S. Kim, *J. Phys. Soc. Jpn.* **70**, 3129 (2001)
17. A.K. Jonscher, *Dielectric Relaxation in Solids* (Chelsea Dielectric Press, London, 1983)
18. D.K. Mahato, A. Dutta, T.P. Sinha, *Mat. Res. Bull.* **47**, 4226 (2012)
19. A. Dutta, T.P. Sinha, *Mat. Res. Bull.* **46**, 518 (2011)
20. S. Summerfield, *Philos. Mag. B* **52**, 9 (1985)
21. N. Balkan, P.N. Batcher, W.R. Hogg, A.R. Long, S. Summerfield, *Philos. Mag. B* **51**, 7 (1985)